Crystal Structure of the von Willebrand Factor Modulator Botrocetin†

Udayaditya Sen,# Sona Vasudevan,# Gowtham Subbarao, Richard A. McClintock, Reha Celikel, Zaverio M. Ruggeri,‡ and Kottayil I. Varughese*,‡

Roon Research Center for Arteriosclerosis and Thrombosis, Division of Experimental Hemostasis and Thrombosis, Department of Molecular and Experimental Medicine and Department of Vascular Biology, The Scripps Research Institute, La Jolla, California 92037

Received September 14, 2000; Revised Manuscript Received November 2, 2000

ABSTRACT: The binding of von Willebrand factor (vWF) to the platelet receptor, glycoprotein (GP) Ib-IX-V complex, has a key role in the initiation of thrombus formation and is regulated by interactions with extracellular matrix components under the influence of hemodynamic forces. To a certain extent, these effects can be mimicked in vitro by two nonphysiologic modulators, ristocetin and botrocetin. The latter, isolated from the venom of the snake *Bothrops jararaca*, is a 31-kDa heterodimeric protein that forms a soluble complex with vWF. As an initial step toward understanding the mechanisms that regulate vWF function, we have solved the crystal structure of botrocetin at 1.8 Å resolution. Botrocetin exhibits homology with other snake proteins, but contains only one metal binding site as compared to two in Factor IX binding protein and Factor IX/X binding protein and none in flavocetin. A distinctive feature of botrocetin is the presence of a negatively charged surface that may play a role in the association with the vWF A1 domain.

Botrocetin, initially described as venom coagglutinin (*1*), is a protein that causes platelet agglutination and aggregation with the involvement of von Willebrand factor (vWF)[1] as a necessary cofactor. In this process, botrocetin and vWF form a bimolecular complex that is then capable of binding specifically to glycoprotein (GP) Ibα (*2*−*4*), a component of the GP Ib-IX-V complex on the platelet membrane (*5*). The venoms of several snake species in the genus *Bothrops* and at least one species in the genus *Bitis* contain an activity with the properties ascribed to botrocetin (*1*), but detailed studies have been conducted mostly with the protein isolated from *Bothrops jararaca* (*6*, *7*). Two chemically distinct forms of botrocetin have been described to date, a disulfide-linked heterodimer of two homologous but distinct polypeptides and a single-chain molecule (*6*, *7*). The former binds to vWF with considerably greater affinity than the latter, but the resulting complexes bind equally well to GP Ibα (*6*). Thus, the variable levels of botrocetin-like activity detected in the venoms of different snakes (*1*) are likely to be the attribute of distinct, albeit possibly related, molecules. The specific binding site for two-chain botrocetin has been identified in the vWF A1 domain (*2*, *8*) and appears to be formed by residues in discontinuous sequence (*9*).

No measurable interaction occurs between normal human vWF in solution and platelet GP Ib-IX-V unless exogenous modulators, such as botrocetin and ristocetin (*10*, *11*), are added or shear stress is applied (*12*). In conditions that mimic more closely pathophysiologic events in circulating blood, immobilized vWF is sufficient, and strictly required at higher shear rates, to mediate rapid and efficient tethering of platelets to reactive surfaces (*13*, *14*). This interaction between vWF and GP Ibα is transient and by itself can only support platelet rolling at low velocity, but by promoting an initial arrest it allows the formation of synergistic bonds involving other receptors that rapidly establish permanent platelet adhesion (*14*). Botrocetin influences this process and, when complexed to vWF, permits firm platelet adhesion mediated only by GP Ibα (*15*). The ability to stabilize the bond between vWF A1 domain and GP Ibα makes botrocetin an important tool for studies aimed at elucidating the three-dimensional conformation of the latter complex and understanding the regulation of vWF function. As a step toward these goals, we have crystallized the disulfide-linked heterodimeric form of botrocetin and solved its structure at 1.8 Å resolution.

EXPERIMENTAL PROCEDURES

Crystallization. Botrocetin was purified from lyophilized crude snake venom (Sigma) following previously published procedures (*4*, *6*, *9*). The purified protein was concentrated to 12 mg/mL in 10 mM ammonium acetate buffer, pH 6.8. Crystals were grown by hanging drop vapor diffusion technique at 22 °C. In a typical experiment, 2 μL of the purified protein was mixed with an equal volume of reservoir

† This work was supported in part by National Institutes of Health Grants HL-55375 and GM54246 (to K.I.V.), HL-31950, HL-42846, and HL-48728 (to Z.M.R.). Sona Vasudevan was the recipient of an International Human Frontier Science Program Long Term Fellowship, and was partly supported by a Skagg Fellowship of The Scripps Research Institute. Additional support was provided by the Stein Endowment Fund and by National Institutes of Health Grant RR0833 to the General Clinical Research Center of Scripps Clinic and Research Foundation.

* Address correspondence regarding this manuscript to Kottayil I. Varughese, The Scripps Research Institute, MEM-116, 10550 N. Torrey Pines Road, La Jolla, CA 92037. Telephone: 858-784-7945. Fax: 858-784-7966. E-mail: kiv@scripps.edu.

# These authors contributed equally to the paper.

‡ Joint senior authors.

[1] Abbreviations: vWF, von Willebrand factor; GP, glycoprotein; PEG, poly(ethylene glycol); PDB, Protein Data Bank; IX-BP, coagulation factor IX-binding protein; IX/X-BP, coagulation factor IX/X-binding protein; rms, root-mean-square.

10.1021/bi0021737 CCC: $20.00
Published on Web 12/15/2000

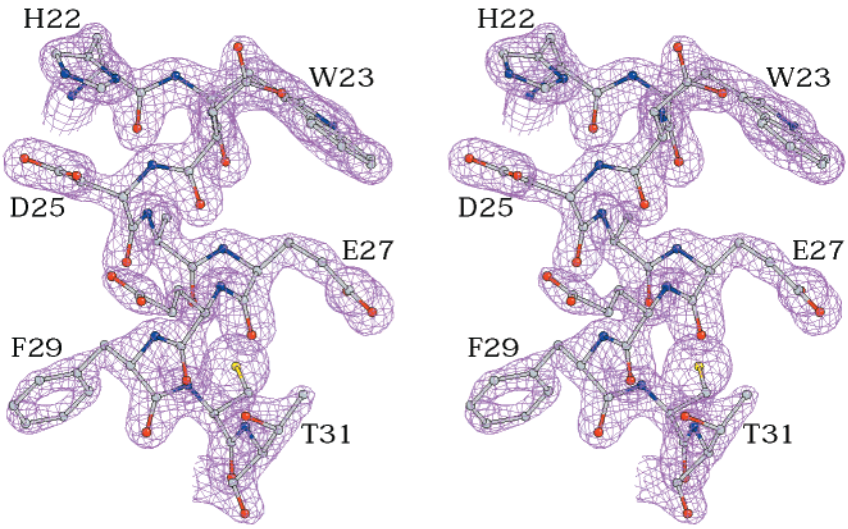

FIGURE 1: A 2Fo−Fc map of a representative portion of botrocetin. Residues 22−31 of the B-chain are shown, and some are identified with the one-letter notation for amino acids. The map is contoured at the 2.1σ level. Produced by Bobscript (*27*).

Table 1: Data Collection and Refinement Statistics

Data Collection	
space group	$P2_12_12_1$
maximum resolution (Å)	1.8
no. of measured reflections	192 473
no. of unique reflections	43 228
completeness overall (%)	97.8
completeness in the highest shell 1.83−1.8 Å (%)	85.4
R_{sym} (%)	4.5
I/σ at the highest shell	3.0
Structure Refinement	
resolution range	50−1.8
reflections	
$F \geq 2\sigma$	38 784
all reflections	43 228
no. of protein atoms	4162
no. of water molecules	603
Mg^{2+} ion	2
R factor (%)	
$F \geq 2\sigma$	19.9 (21.8)[a]
all reflections	21.8 (23.9)
rmsd from ideal bond lengths (Å)	0.006
rmsd from ideal bond angles (deg)	1.4

[a] Values in parentheses are for R_{free}.

solution containing 8% poly(ethylene glycol) (PEG) 4000, 14% PEG 400, and 100 mM $MgCl_2$ in 100 mM Tris-HCl buffer, pH 8.5. Crystals appeared within 2−3 days. The crystals belonged to space group $P2_12_12_1$, with unit cell dimensions a = 64.8, b = 69.7, and c = 103.5 Å. The asymmetric unit contained two heterodimeric molecules of botrocetin, with V_m = 1.98 corresponding to a solvent content of 35%.

Data Collection. Crystals were frozen in a stream of nitrogen (Oxford Cryosystem) at 100 K after a brief soaking in 30% PEG 400 as cryoprotectant. Diffraction data to a resolution of 1.8 Å were collected at the Stanford Synchrotron Radiation Laboratory, beamline BL9-2 using an ADSC CCD detector with a crystal-to-detector distance of 220 cm at a wavelength of 0.98 Å. One hundred and thirty-five images were collected with a 1° rotation for each frame. The data were processed using the programs Denzo (*16*) and Scalepack (*17*). There was a total of 43 228 unique reflections, with an overall R_{sym} of 4.5% and completeness of 97.8% at a resolution of 1.8 Å (Table 1).

Structure Solution. The structure was solved by molecular replacement using the program AmoRe (*18*) implemented in the Collaborative Computational Project Number 4 (CCP4) suite of programs (*19*). The A-chain of coagulation factor IX-binding protein (IX-BP; PDB entry 1BJ3) and the B-chain of coagulation factor IX/X binding protein (IX/X-BP; PDB entry 11XX) were chosen as search models based on higher sequence homology and better resolution. A common feature among these proteins is the existence of a long loop comprising about 25 residues involved in loop swapping dimerization (*20*). As this loop exhibits conformational flexibility, it was deleted from the search models. Initial rotation and translational searches for the A-chain yielded several solutions with a similar correlation coefficient and R factor. The two correct solutions, however, could only be identified after rigid body refinements. After positioning the two A-chains in the unit cell, the two B-chains were located by similar procedures, and the packing of the four polypeptides in the unit cell was inspected graphically. The correlation coefficient and R factor at this stage were 37.4 and 48.7%, respectively, for data in the resolution range of 15 to 3.5 Å.

Refinement. All crystallographic refinements were carried out using the program CNS (*21*), and the progress of refinement was monitored by calculating the value of R_{free} from a randomly selected set containing 5% of the total reflections. A σ_A-weighted 2|Fo|−|Fc| electron density map at 3.5 Å was calculated, and some preliminary adjustments in the model were carried out. The resolution of the map was extended gradually to 2.5 Å using the maximum likelihood method as implemented in CNS. After two cycles of positional refinements, followed by model building, the R factor dropped to 40% (R_{free} = 43%). Several cycles of positional refinements and model building were then performed, progressively increasing the resolution at each step to include all data at 1.8 Å, with an R factor of 34.6% (R_{free} = 37.1%). The electron density map at this stage revealed the positions of most of the residues in the long loop that were deleted from the search models. All amino acid residues from both chains were built into the density, with the exception of four residues (Asp^{88}−Tyr^{91}) of the B-chain that were not visible. One Mg^{2+} ion bound to the B-chain of each

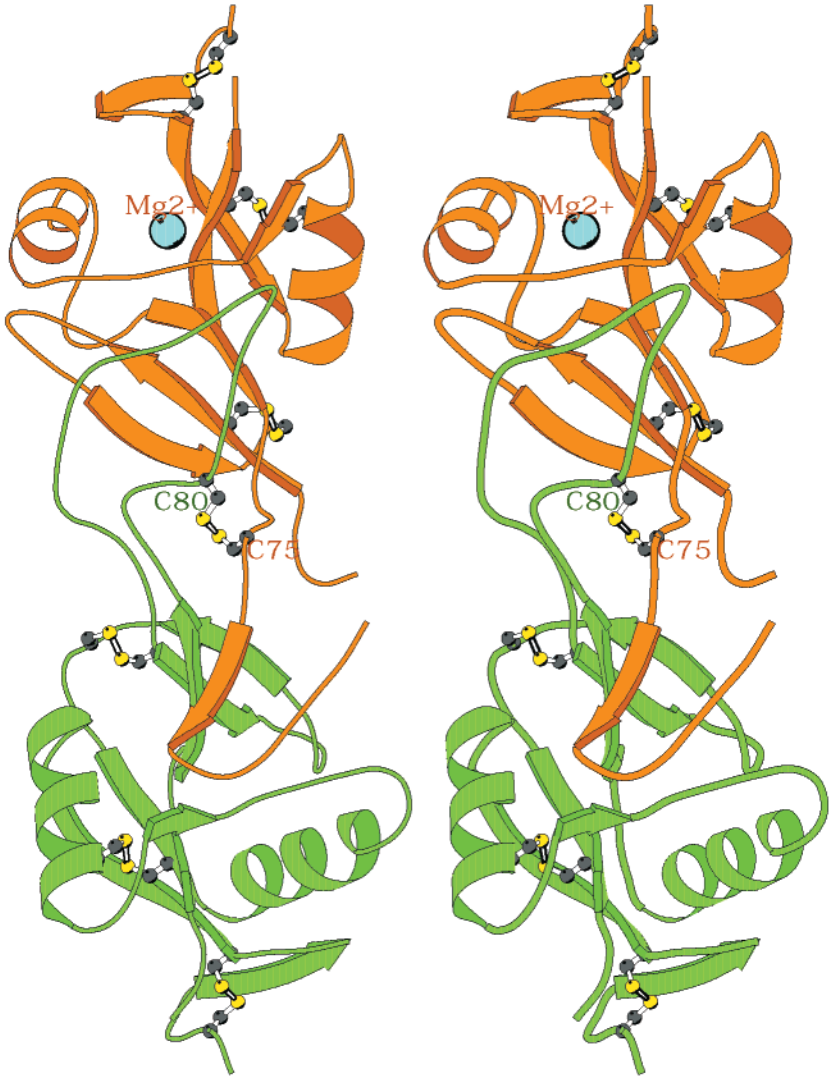

FIGURE 2: Stereoview of the botrocetin molecule. The A-chain is shown in green, the B-chain is shown in orange and Mg^{2+} is shown in cyan. Disulfide bridges are shown as ball-and-stick. There are six intrachain disulfide bridges (Cys^{2}−Cys^{13}, Cys^{30}−Cys^{128}, Cys^{103}−Cys^{120} in the A-chain; Cys^{2}−Cys^{13}, Cys^{30}−Cys^{121}, Cys^{98}−Cys^{113} in the B-chain) and one interchain disulfide bridge (Cys^{80} of the A-chain and Cys^{75} of the B-chain). Produced by Bobscript (*27*).

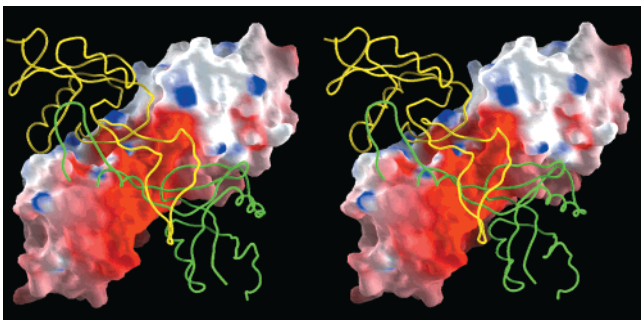

FIGURE 3: Stereoview of botrocetin tetramers as seen in the crystal lattice. One dimer is shown by a surface representation, the other is shown by a wire model with the A-chain in yellow and the B-chain in green. Produced by GRASP (*28*).

molecule also became apparent. Individual B factor refinements reduced the R factor to 23.9% (R_{free} = 26.2%). Water molecules were added to the model using the program WATERPICK implemented in the CNS suite of programs. The criteria used to assign a water molecule were that it had electron density greater than 3σ in the Fo−Fc map, and more than 1σ in 2Fo−Fc map, in addition to forming at least one hydrogen bond with a protein atom. The final model[2] was refined to an R factor of 19.9% (R_{free} = 22.1%) for data between 50 and 1.8 Å. The stereochemistry of the final model was examined by PROCHECK. The statistics of refinement are listed in Table 1.

RESULTS AND DISCUSSION

Overall Architecture. A representative portion of the electron density (Figure 1) demonstrates the quality of the three-dimensional model of botrocetin obtained with these X-ray crystallography studies. The electron density for residues Asp^{88}−Tyr^{91} of the B-chain, however, was of poor quality, possibly because of high conformational flexibility, and these residues have not been included in the final model. The most favored region of the Ramachandran plot contains 91% non-glycine and non-proline residues, with the rest in additionally allowed regions. The root-mean-square (rms) deviations for bond length and bond angles are 0.006 Å and 1.40°, respectively, with average B factor for protein and

[2] The atomic coordinates of the model have been deposited with the PDB under the accession number 1FVU.

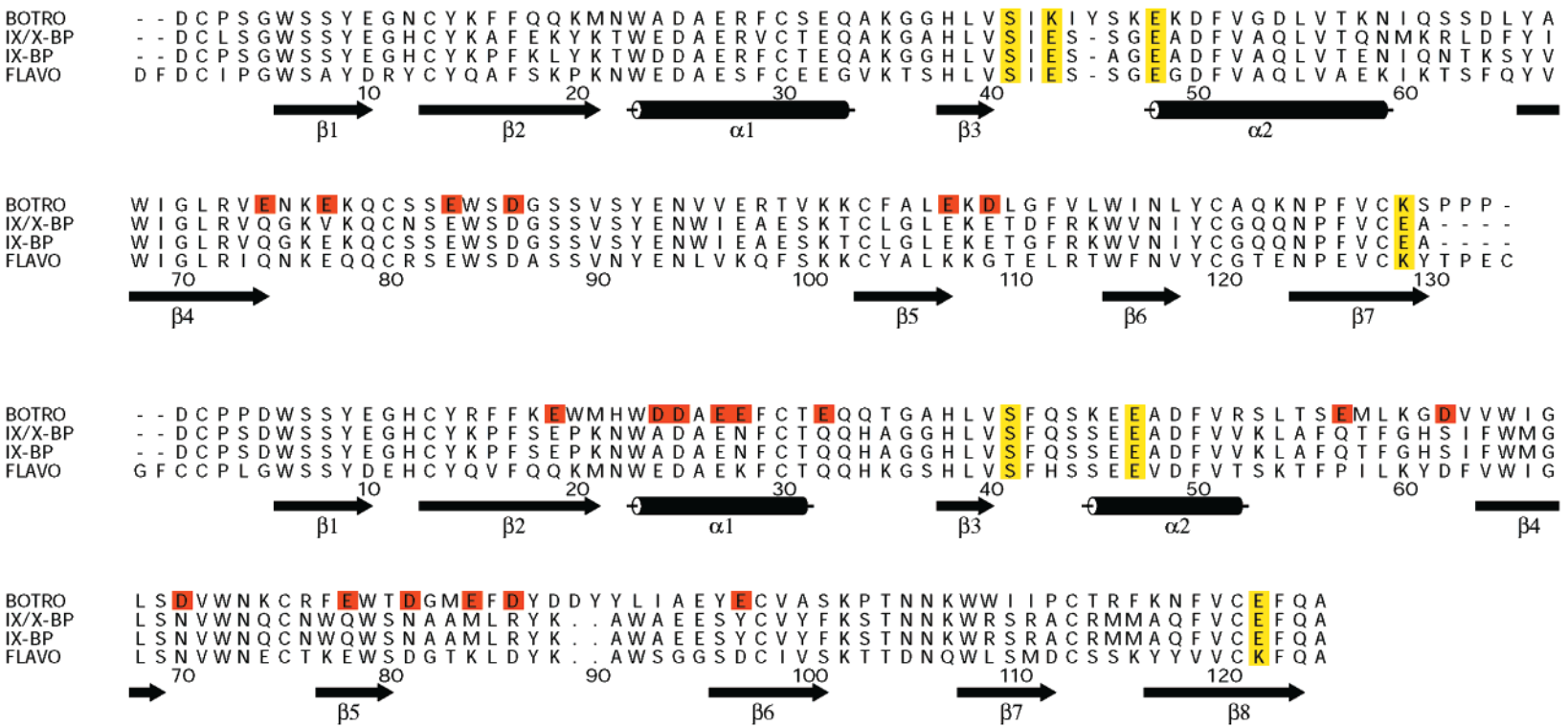

FIGURE 4: Structure-based sequence alignment of botrocetin (botro) with coagulation factor IX/X-BP, coagulation factor IX-BP, and flavocetin (flavo). Top, A-chain; bottom, B-chain. Secondary structures are indicated under the sequences. The residues that occupy positions potentially involved in the coordination of metal binding are shown in yellow, and the residues that form the acidic surface of botrocetin are shown in red. Coagulation factor IX/X-BP and coagulation factor IX-BP have one metal binding site in each chain. Botrocetin has one metal binding site in the B-chain; the one in the A-chain is lost owing to two Glu-to-Lys substitutions. Both sites are lost in flavocetin owing to a Glu-to-Lys and a Gln-to-His substitutions. Produced by Alscript (*29*).

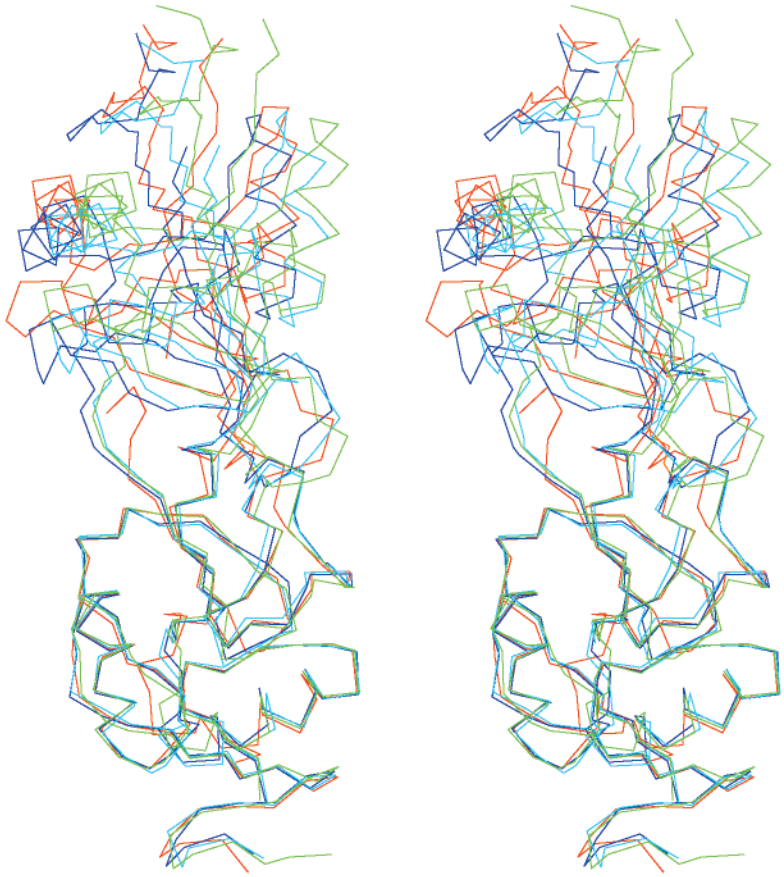

FIGURE 5: Superposition of the B-chains of coagulation factor IX/X-BP, coagulation factor IX-BP, and flavocetin with that of botrocetin. Botrocetin is shown in red, flavocetin is shown in green, coagulation factor IX/X-BP is shown in blue, and coagulation factor IX-BP is shown in sky blue. The interchain disulfide bond of botrocetin is shown in orange. Produced by Insight (release 95.0; Biosym/Molecular Simulations Inc.).

water of 33.9 and 41.8 Å^2, respectively. The average error in the coordinates of the model, as estimated from Cruickshank's formula (*22*), is 0.24 Å. The overall three-dimensional fold of botrocetin is very similar to that of several other snake venom proteins that belong to the C-type lectin super family, which includes coagulation factor IX-BP, coagulation factor IX/X-BP, and flavocetin. Despite a similar fold, these proteins have varied functions and specificities.

Botrocetin is a disulfide-linked heterodimer composed of two homologous chains, A and B (Figure 2). The botrocetin heterodimer is an elongated molecule with overall dimensions of ~75 × 35 × 35 Å. Each subunit has a compact globular unit and an extended long loop. The globular domain consists of two α-helices and five major β-strands. The long loop protrudes from this globular unit and is involved in extensive interactions with the globular domain of the other subunit to form a loop-exchange dimer. Cys^{80} from the A-chain and Cys^{75} from the B-chain form an interchain disulfide bridge (Figure 2). The botrocetin dimer has a concave surface in the middle, thus two dimers can associate tightly in the form of a cross and this efficient packing contributes to the low solvent content (35%). Indeed, the asymmetric unit contains two molecules that associate in the crystal lattice to form a tetramer (Figure 3). Upon association, 10% of the surface area of the dimer gets buried at the interface. The association in the crystal lattice is primarily driven by hydrophilic interactions, hence separation into individual dimers can easily occur in solution. The two molecules have exactly the same conformation, and the main chain Cα atoms superpose with an rms deviation of 1.0 Å.

Comparison with Other Heterodimers in the C-Type Lectin Superfamily. Both chains of botrocetin are homologous to carbohydrate recognition domains (CRD) of C-type lectin superfamily members. In the C-type lectins, the long loop folds back to the globular domain, while in botrocetin it extends to the adjoining domain to form a loop swapping dimer as seen in IX/X-BP (*20*). The loop of the A-chain is thus involved in extensive interactions with the globular domain of the B-chain and vice versa. It has been proposed that loop swapping leads to loss of carbohydrate-binding activity (*20*). Botrocetin is structurally similar to three other heterodimeric proteins of the C-type lectin superfamily, i.e., coagulation factor IX/X-BP, coagulation factor X-BP, and the GP Ib-binding protein, flavocetin. All these proteins share a high degree of sequence similarity (Figure 4). A comparison of the three-dimensional structures of both A and B chains of botrocetin with the respective chains of the other three proteins reveals that only minor local differences exist among them, which are mainly due to insertions/deletion of residues. Despite the close similarity of the individual chains, the relative orientation between the two chains is different in botrocetin as compared to the other three proteins, a fact that can be appreciated when the B-chains are superposed (Figure 5). The position of the interchain disulfide bond acts as a pivot point about which the A-chain moves. The

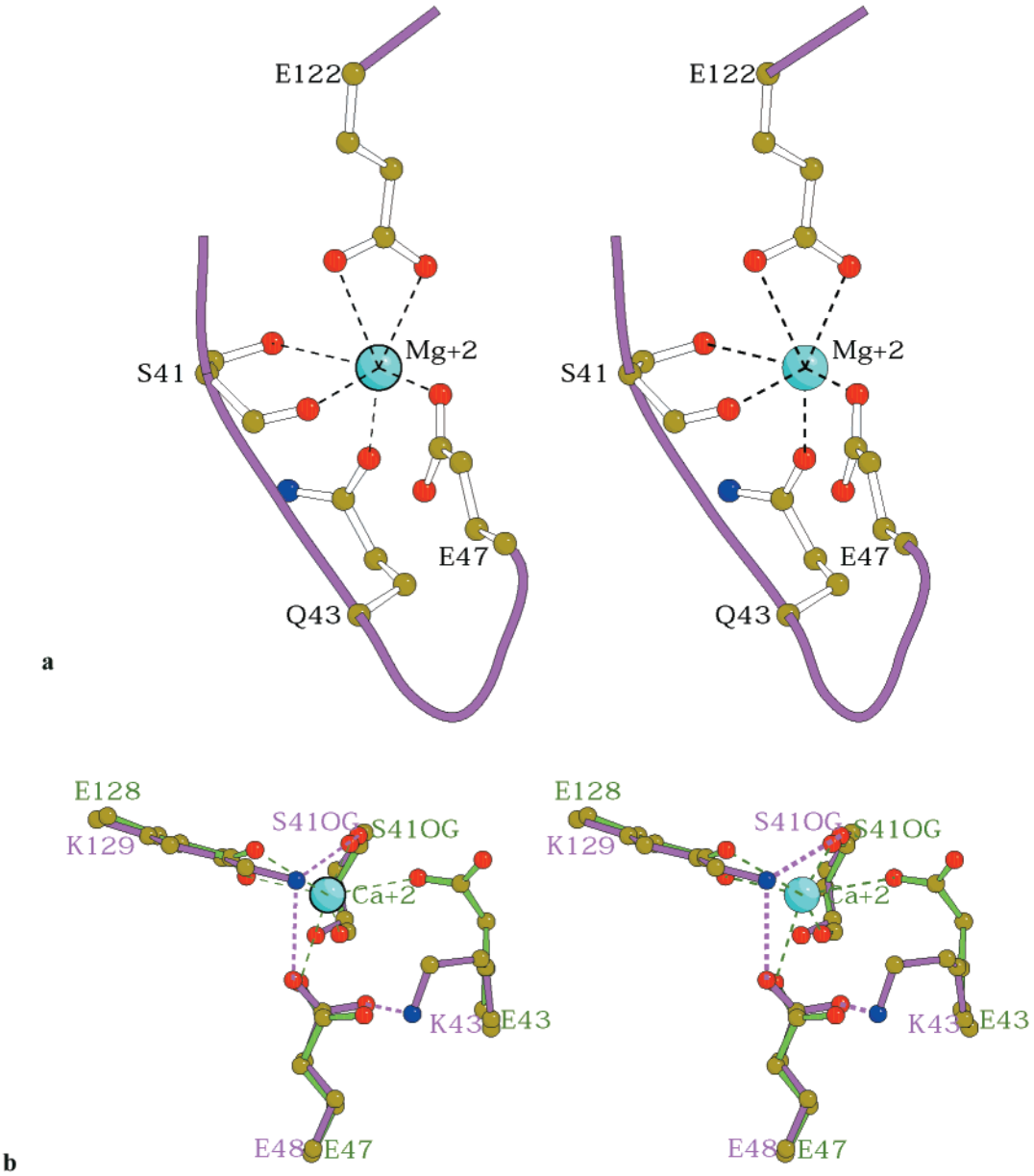

FIGURE 6: Metal ion coordination sites. (a) Metal ion coordination in the B-chain of botrocetin. (b) Superposition of the metal ion coordination site in A-chain of coagulation factor IX/X BP (in green) with the corresponding site in botrocetin (in magenta), which does not bind metal. Metal ion is shown in blue. Produced by Bobscript (*27*).

B-chains of coagulation factor IX/X-BP and coagulation factor X-BP are identical in sequence, while the B-chain of botrocetin is markedly different. The homology of the A chain with the other three proteins is ~61%, while that of the B chain is only ~52%. The greater degree of variability in the sequence suggests that the B-chain may be primarily responsible for the unique functional specificity of botrocetin. Indeed, as dicussed below, our results indicate that the B-chain is the major contributor to the proposed vWF A1 domain binding surface.

Intersubunit Interface. Dimerization is accomplished through loop swapping, and it is dominated by hydrophobic interactions between the swapped loop and the globular unit. Residues involved in these hydrophobic interactions are highly conserved among members of the C-type lectin superfamily. This interface is known as the C-interface. The A and B chains are linked through a disulfide bridge, but the association is driven by interactions at the C-interface. For example, rhodocetin, a platelet aggregation inhibitor (*23*), can dimerize even though it lacks an interchain disulfide bridge.

Metal Binding Site. One divalent metal binding site in the B-chain of botrocetin (Figure 6, panel a) is similar to that seen in both coagulation factor IX/X-BP and coagulation factor IX-BP. As discussed in Experimental Procedures, crystals of botrocetin were obtained in the presence of 100 mM $MgCl_2$. In addition, the electron density and coordination geometry of the metal present in botrocetin corresponded to those of a Mg^{2+} ion; therefore, the assignment was unambiguous. The side chains of residues Ser^{41}, Gln^{43}, Glu^{47}, and Glu^{122} in the B-chain coordinate with the Mg^{2+} ion. At variance with the metal ion binding site in coagulation factor IX-BP, we found no water molecule within the Mg^{2+} ion coordination sphere; instead, both Oδ1 and Oδ2 atoms of Glu^{47} coordinate with the Mg^{2+} ion in botrocetin. There is no bound divalent metal ion in the A-chain of botrocetin,

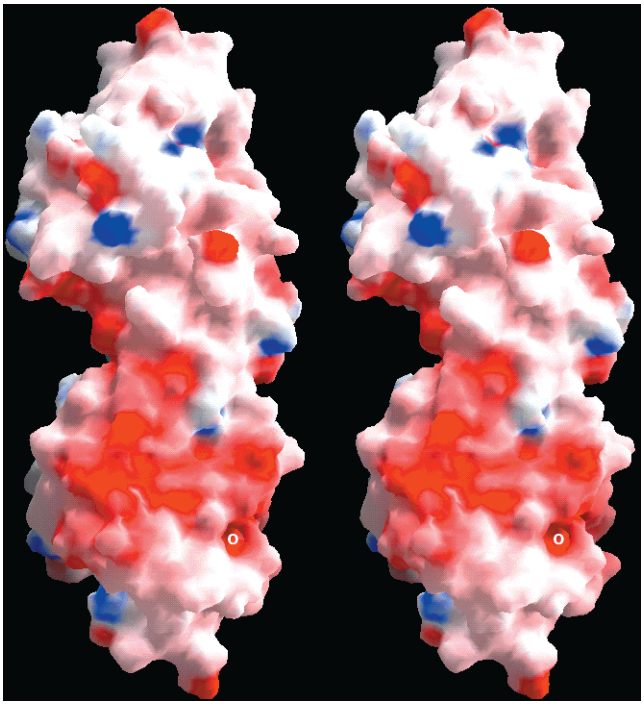

FIGURE 7: Representation of the botrocetin heterodimer showing the surface charge distribution. The position of magnesium is shown as o(white). The acidic surface of the molecule is shown in red. Produced by GRASP (*28*).

unlike in the homologous chains of coagulation factor IX/X-BP and coagulation factor IX-BP. The loss of this metal ion binding site in botrocetin is due to specific amino acid substitutions (Figure 4 and Figure 6, panel b). Residues corresponding to Ser^{41} and Glu^{47} of coagulation factor IX/X-BP and coagulation factor IX-BP are conserved (residues Ser^{41} and Glu^{48} of botrocetin), but residues corresponding to Glu^{43} and Glu^{128} in the former two proteins are replaced by Lys^{43} and Lys^{129} in botrocetin, giving rise to a positive charge instead of a negative charge. With these changes, the overall charge−charge interactions in the absence of divalent metal ion are maintained (Figure 6, panel b). In botrocetin, the Nζ atom of Lys^{129} is spatially close to the position corresponding to the Mg^{2+} ion in coagulation factor IX/X-BP and coagulation factor IX-BP and forms a hydrogen bond with Ser^{41} and Oδ1 of Glu^{48}, while the Nζ atom of Lys^{43} forms a hydrogen bond with Oδ2 of Glu^{48}.

The significance of these substitutions in the A-chain of botrocetin, or even the relevance of the bound metal in the B-chain, are not known, but similar structural changes have been observed in other molecules. For example, phosphotransfer reactions normally require the presence of cations such as Mg^{2+}. The prevailing notion is that the metal neutralizes the charges on the phosphoryl oxygens to stabilize the transition state intermediate. Recently, it was observed that the histidine kinase EnvZ, which normally requires cations for autophosphorylation, can do so in the absence of cations (*24*) if a Thr residue in the vicinity of the phosphorylation site is changed to an arginine. This observation suggests that the guanidinium group may substitute for the cation. It should be noted that the ability of botrocetin to induce vWF binding to GP Ib (*4*) and platelet agglutination (*1*) is not affected by the presence of EDTA.

The Acidic Surface of Botrocetin in Relation to Binding of the vWF A1 Domain. A comparison of the surface potential of botrocetin with that of coagulation factor IX/X-BP and coagulation factor IX-BP shows some interesting differences that may explain the distinct functional properties of each molecule. The two coagulation factor-binding proteins exhibit a positively charged patch near their concave surface that is thought to be required for interaction with the γ-carboxyl glutamic acid (Gla) residues in factors IX/X-BP and IX-BP (*20*). In botrocetin, this positive charge is changed due to the substitution of three Arg residues with Trp, Ile, and Thr. On the other hand, polar residues considered as possible candidates for GP Ib binding in flavocetin (*25*) are not the same in botrocetin. The latter has a very markedly acidic surface (Figure 7), comprising mainly residues in the B-chain, located near the concave face of the molecule and connected to the metal binding site. The 20 acidic residues (14 from the B-chain and 6 from the A-chain) that form the negatively charged cleft in botrocetin (Figure 7) are substituted in the other three proteins mostly by nonacidic, polar and noncharged residues (Figure 4). In coagulation factor IX/X-BP and IX-BP, seven of them are retained as acidic residues and one is switched to a basic residue. In flavocetin, 10 remain acidic and three change to basic residues. This negative surface in botrocetin is likely to be involved in binding to a positive region of the vWF A1 domain, since recent studies have identified A1 domain residues Arg^{629}, Arg^{632}, Arg^{636}, and Lys^{667} as putative binding sites for botrocetin (*26*). Apart from the concentration of negative charges, another feature that makes botrocetin distinct from the other three proteins is the change in the shape of the binding surface. This is caused mainly by a change in the relative orientation between A and B chains and by the insertion of residue 45 in the A-chain and residues 89 and 90 in the B-chain (Figure 4). The latter are in the extended loop and contribute to the negative charge on the surface.

ACKNOWLEDGMENT

We thank Jerry Ware for helpful discussion and Rachel Braithwaite for secretarial assistance.

REFERENCES

1. Read, M. S., Shermer, R. W., and Brinkhous, K. M. (1978) *Proc. Natl. Acad. Sci. 75*, 4514−4518.
2. Fujimura, Y., Holland, L. Z., Ruggeri, Z. M., and Zimmerman, T. S. (1987) *Blood 70*, 985−988.
3. Read, M. S., Smith, S. V., Lamb, M. A., and Brinkhous, K. M. (1989) *Blood 74*, 1031−1035.
4. Andrews, R. K., Booth, W. J., Gorman, J. J., Castaldi, P. A., and Berndt, M. C. (1989) *Biochemistry 28*, 8317−8326.
5. Ware, J. (1998) in *Von Willebrand Factor and the Mechanisms of Platelet Function* (Ruggeri, Z. M., Ed.) pp 111−139, Springer, Berlin.
6. Fujimura, Y., Titani, K., Usami, Y., Suzuki, M., Oyama, R., Matsui, T., Fukui, H., Sugimoto, M., and Ruggeri, Z. M. (1991) *Biochemistry 30*, 1957−1964.
7. Usami, Y., Fujimura, Y., Suzuki, M., Ozeki, Y., Nishio, K., Fukui, H., and Titani, K. (1993) *Proc. Natl. Acad. Sci. 90*, 928−932.
8. Shelton-Inloes, B. B., Titani, K., and Sadler, J. E. (1986) *Biochemistry 25*, 3164−3171.
9. Sugimoto, M., Mohri, H., McClintock, R. A., and Ruggeri, Z. M. (1991) *J. Biol. Chem. 266*, 18172−18178.

10. Howard, M. A., and Firkin, B. G. (1971) *Thromb. Haemost. 26*, 362−369.
11. Kao, K. J., Pizzo, S. V., and McKee, P. A. (1979) *J. Clin. Invest. 63*, 656−664.
12. Goto, S., Salomon, D. R., Ikeda, Y., and Ruggeri, Z. M. (1995) *J. Biol. Chem. 270*, 23352−23361.
13. Savage, B., Saldivar, E., and Ruggeri, Z. M. (1996) *Cell 84*, 289−297.
14. Savage, B., Almus-Jacobs, F., and Ruggeri, Z. M. (1998) *Cell 94*, 657−666.
15. Miyata, S., and Ruggeri, Z. M. (1999) *J. Biol. Chem. 274*, 6586−6593.
16. Otwinowski, Z., and Minor, W. (1997) *Methods Enzymol. 276*, 307−326.
17. Gewirth, D. (1993) *The Denzo Manual*, Yale University and Howard Hughes Medical Institute, Department of Molecular Biophysics & Biochemistry, New Haven, CT.
18. Navaza, J. (1994) *Acta Crystallogr. A 50*, 157−163.
19. Collaborative Computational Project, Number 4. (1994) *Acta Crystallogr. D50*, 760−763.
20. Mizuno, H., Fujimoto, Z., Koizumi, M., Kano, H., Atoda, H., and Morita, T. (1997) *Nat. Struct. Biol. 4*, 438−441.
21. Brunger, A. T., Adams, P. D., Clore, G. M., DeLano, W. L., Gros, P., Grosse-Kunstleve, R. W., Jiang, J. S., Kuszewski, J., Nilges, M., Pannu, N. S., Read, R. J., Rice, L. M., Simonson, T., and Warren, G. L. (1998) *Acta Crystallogr. D54*, 905−921.
22. Cruickshank, D. W. J. (1999) *Acta Crystallogr. D55*, 583−601.
23. Wang, R., Kini, R. M., and Chung, M. C. (1999) *Biochemistry 38*, 7584−7593.
24. Dutta, R., Yoshida, T., and Inouye, M. (2000) *J. Biol. Chem. 275*, 38645−38653.
25. Fukuda, K., Mizuno, H., Atoda, H., and Morita, T. (2000) *Biochemistry 39*, 1915−1923.
26. Matsushita, T., Meyer, D., and Sadler, J. E. (2000) *J. Biol. Chem. 275*, 11044−11049.
27. Esnouf, R. M. (1997) *J. Mol. Graph. Model. 15*, 132−134.
28. Nicholls, A., Bharadwaj, R., and Honig, B. (1993) *Biophys. J. 64*, 166−169.
29. Barton, G. J. (1993) *Protein Eng. 6*, 37−40.

BI0021737